Control, Simulation and Validation of a Hybrid Actuator for a Maglev Train Model on a Scale of 1:20

Jan Philipp Rickwärtz, Johann Kolb and Kay Hameyer, *Senior Member, IEEE*
Institute of Electrical Machines (IEM)
RWTH Aachen University
Aachen, Germany
jan.rickwaertz@iem.rwth-aachen.de

2020 21st International Conference on Research and Education in Mechatronics (REM) | 978-1-7281-6224-9/20/$31.00 ©2020 IEEE | DOI: 10.1109/REM49740.2020.9313869

***Abstract*—Hybrid actuators combine permanent magnet and electromagnetic forces, leading to highly energy-efficient operation. With a sophisticated design, only dynamic air gap deviations have to be compensated.**
Hybrid actuators have an inherently unstable system behavior. This paper presents an approach for designing a current and air gap controller to achieve dynamic stability. This is realized by adding a PID-controller to the mechanical system in such a way, that the resulting system can be described by a damped harmonic oscillator. The desired system behavior is achieved by adjusting the characteristics of the spring-damper-element with the controller parameters.
Subsequently, the actuator is simulated with the calculated parameters and a prototype on a scale of 1:20 is tested in the laboratory. With the applied controller design the measurements show a considerable accordance.

***Index Terms*—controller design, electromagnetic levitation, hybrid actuator, maglev train.**

I. Introduction

Based on their working principle, Maglev trains can reach high speed and are therefore suitable for transportation over long distances in a short period of time. With increasing efficiency and decreasing costs for power electronics as well as strongly increasing computing performance of microcontrollers, it is possible to integrate the linear motor and the magnetic levitation system in the train. Previous works have discussed the electromagnetic levitation [1], [2] and controlling of a levitation system equipped with permanent magnets [3].
To reduce the power loss for levitation, the actuator consists of coils and permanent magnets. The magnets are designed in such a way, that they compensate a static load. Additional electromagnetic force is only needed for the levitation and guidance control to compensate additional load.
In the first section of this paper the theory and design of the actuator is outlined. In the second section the controller design is discussed to reach dynamic stability. In the last section the prototype is measured on a test bench and the simulation is compared to measurement results.

II. Theory of Electromagnetic Levitation

The concept of hybrid actuators is based on electromagnetic suspension (EMS). NdFeB-magnets are used to provide static magnetic forces strong enough to lift Maglev trains against its own weight force. Dynamic stability is reached by adding coils controlled by power electronics leading to adjustable electromagnetic forces.

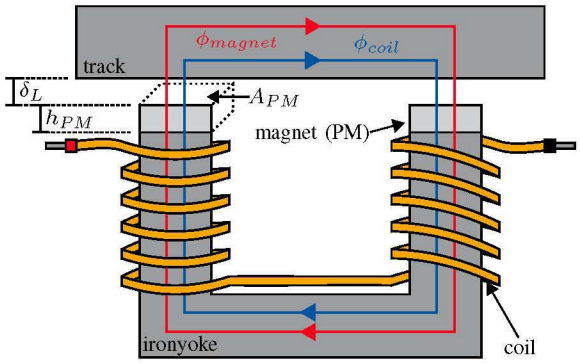

Fig. 1: Magnetic circuit of hybrid actuator.

The magnetic circuit in Fig. 1 consists of an iron yoke, two NdFeB-magnets assembled on top of the yoke and a coil devided into two parts on the legs of the yoke. The circuit is closed by an adjustable air gap and the track. Calculation of magnetic forces in the magnetic circuit is based on Ampère's law, where H is the magnetic field strength and Θ is the magnetomotive force

$$\oint \vec{H} \cdot d\vec{s} = \Theta \,. \tag{1}$$

The magnetic circuit can be divided into areas of constant magnetic field strength and the respective mean length of path of yoke ($H_{FE},\ l_{FE}$), air gaps ($H_{air},\ \delta_L$) and magnets ($H_{PM},\ h_{PM}$)

$$N \cdot I = H_{Fe} \cdot l_{Fe} + 2 \cdot H_{PM} \cdot h_{PM} + 2 \cdot H_{air} \cdot \delta_L \,, \tag{2}$$

where N is the total number of turns of the coil and I is the current through the coil.
The flux density of the magnets B_{PM} is determined by the remanence B_R and the external magnetic field strength H_{PM}. With the magnetic field constant μ_0 and relative permeability $\mu_{r,PM}$ the external flux density can be described as

$$B_{PM} = B_R + \mu_0 \cdot \mu_{r,PM} \cdot H_{PM} \,. \tag{3}$$

978-1-7281-6224-9/20/$31.00 ©2020 IEEE

From (3), the total magnetic field strength in the magnet H_{PM} follows

$$H_{PM} = \frac{B_{PM} - B_R}{\mu_0 \cdot \mu_{r,PM}}. \tag{4}$$

For yoke and air gap, the relation between field strength and flux density can be found from general material equation $B = \mu_0 \cdot \mu_r \cdot H$. Inserting this equation and (3) in (2), dependency on magnetic flux density B follows

$$N \cdot I = \frac{B_{Fe}}{\mu_0 \cdot \mu_{r,Fe}} \cdot l_{Fe} + 2 \cdot \frac{B_{PM} - B_R}{\mu_0 \cdot \mu_{r,PM}} \cdot h_{PM} + 2 \cdot \frac{B_{air}}{\mu_0} \cdot \delta_L. \tag{5}$$

For all following considerations, stray flux is neglected ($B_{Fe} = B_{PM} = B_{air}$) and the relative permeability of iron is assumed to be infinitely high ($\mu_{r,Fe} \to \infty$). This leads to a simplification of equation (5)

$$N \cdot I = 2 \cdot \frac{B_{air} - B_R}{\mu_0 \cdot \mu_{r,PM}} \cdot h_{PM} + 2 \cdot \frac{B_{air}}{\mu_0} \cdot \delta_L \,. \tag{6}$$

The Total force of the hybrid actuator F_{Mag} is given by Maxwell's pulling force formula

$$F_{Mag} = 2 \cdot \frac{B_{air}^2 \cdot A_{PM}}{2 \cdot \mu_0} = \frac{B_{air}^2 \cdot A_{PM}}{\mu_0}. \tag{7}$$

The air gap flux density B_{air} can be derived from (6)

$$B_{air} = \frac{N \cdot I \cdot \mu_0 \cdot \mu_{r,PM}}{2 \cdot (h_{PM} + \delta_L \cdot \mu_{r,PM})} + \frac{B_R \cdot h_{PM}}{h_{PM} + \delta_L \cdot \mu_{r,PM}}. \tag{8}$$

This leads to the total magnetic force F_{Mag} of the hybrid actuator dependent on the current I in the coils and air gap δ_L

$$F_{Mag} = \frac{A_{PM}}{\mu_0} \cdot \left(\frac{N \cdot I \cdot \mu_0 \cdot \mu_{r,PM} + 2 \cdot B_R \cdot h_{PM}}{2 \cdot (h_{PM} + \delta_L \cdot \mu_{r,PM})} \right)^2. \tag{9}$$

III. Design of the Hybrid Actuator

The actuator is designed to carry a defined load at reference air gap only by permanent magnet forces. If the air gap changes due to additional load, a current is applied to set the air gap back to its reference value (see sec. IV).

The applied permanent magnets of the hybrid actuator are NdFeB magnets with a minimum remanence flux density of $B_R = 1.17\,\mathrm{T}$. The height of the magnet is $h_{PM} = 1.0\,\mathrm{mm}$

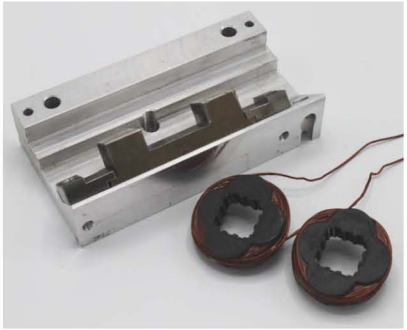

Fig. 2: Disassembled hybrid actuator.

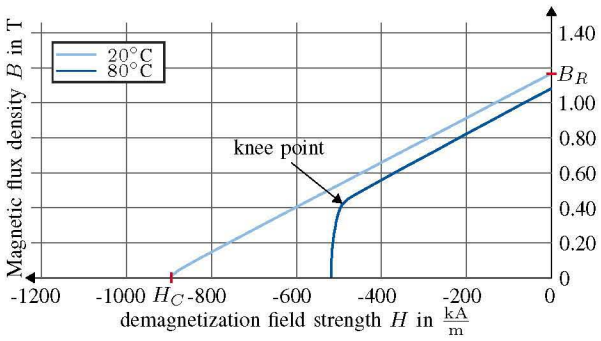

Fig. 3: Demagnetization curve of a NdFeB magnet at different temperatures.

with a surface of $A_{PM} = 400\,\mathrm{mm}^2$ and a permeability of $\mu_{r,PM} = 1.05$. For the track and the train model the reference air gap is set to $\delta_L = 1.0\,\mathrm{mm}$. With the pulling force formula (9) the resulting levitation force of the permanent magnets $F_{Mag,PM}$ can be calculated to

$$F_{Mag}(I = 0\,\mathrm{A}) = F_{Mag,PM} = 103.7\,\mathrm{N}. \tag{10}$$

If the load differs, a positive or negative current is applied to compensate the additional load.

An important aspect for the actuator design is the knee point in the characteristic curve of the permanent magnet in Fig. 3. If the temperature of the coils rises, the knee point of the demagnetization curve shifts towards a higher field strength. If the magnetomotive force coming from the coils impresses a field strength below the field strength at the knee point, the magnet is irreversible demagnetized.

Therefore, the maximum magnetomotive force to derive the maximum allowed negative current has to be calculated. The magnetomotive force can be expressed as

$$\Theta_{max} = -\frac{B_\mathrm{R} - B_\mathrm{min}}{\mu_0 \cdot \mu_{r,PM}} \cdot \left(1 + \frac{\mu_{r,PM} \cdot A_\mathrm{PM}}{A_L}\, \delta_L \right). \tag{11}$$

The formula depends on the air gap δ_L, thus the maximum current has to be calculated every control cycle to not demagnetize the magnets.

The designed coils have $N = 2 \cdot 70$ turns with a wire diameter

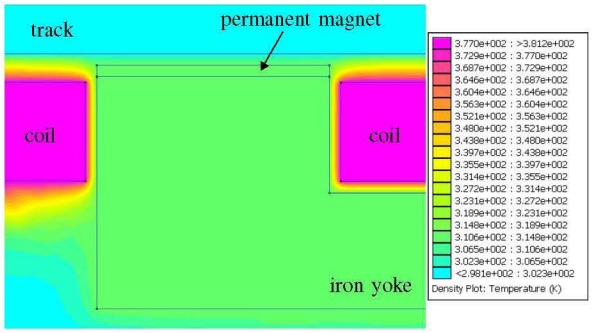

Fig. 4: Temperature rising with a maximum continuous current of 4.6 A after 10 min at a start temperature of 25 °C.

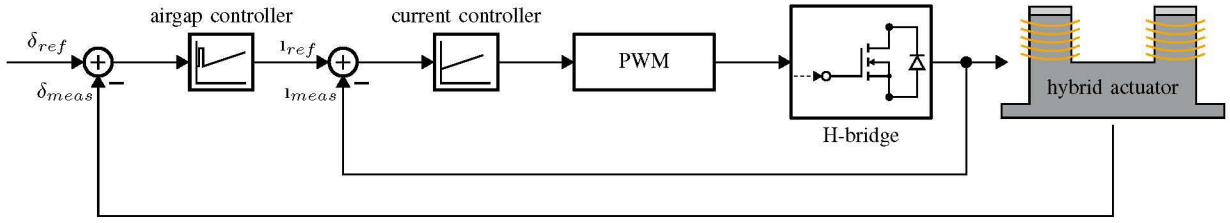

Fig. 5: Block diagram of the control loop.

of $1.024\,\mathrm{mm}$. The yoke is designed in such a way that the coils have sufficient space between each other so that the heat is dissipated. The measured resistance and inductance at $10\,\mathrm{kHz}$ are $R = 1.064\,\Omega$ and $L = 389\,\mu\mathrm{H}$. The expected maximum continuous current is $I = 4.6\,\mathrm{A}$.
To be sure the maximum allowed temperature of $\theta_{max} = 80\,^{\circ}\mathrm{C}$ is not exceeded at the maximum continuous current, a temperature simulation is performed. A time span of $10\,\mathrm{min}$ is simulated, which is more than the expected time span at which the actuator will be operated at maximum continuous current. Fig. 4 shows the corresponding temperature distribution. The magnets will not exceed a temperature of about $42\,^{\circ}\mathrm{C}$, which is sufficient for the continuous operation of the hybrid actuator.

IV. Controller Design

The controller is designed as cascade. The inner loop is a current controller and the outer one the air gap controller. Fig. 5 shows the topology of the controller design.

A. Electrical Subsystem

For the current controller the electric operating principle has to be derived. The differential equation describing the resulting voltage u of the coil can be separated into an ohmic part, described by resistance R and current i and an inductive part, given by the change of flux linkage ψ.

$$u(t) = R\,i(t) + \frac{d}{dt}\psi\left(i, \delta_L\right). \tag{12}$$

With a partial differentiation of $\psi\left(i, \delta_L\right)$ the equation leads to

$$u(t) = R\,i(t) + L\left(\delta_L\right)\frac{di(t)}{dt} - \frac{dL\left(\delta_L\right)}{d\delta_L(t)}\dot{\delta}_L(t)i(t). \tag{13}$$

With the assumption of small air gap changes within one control cycle, the induced voltage generated by position changing is neglected here. With the Laplace Transformation the transfer function is outlined as

$$G_C = \frac{I(s)}{U(s)} = \frac{\frac{1}{R}}{\frac{L}{R}\,s + 1} = \frac{\frac{1}{R}}{T_l\,s + 1}. \tag{14}$$

For the current controller a PI control structure is applied. To evaluate the optimal control parameters the magnitude optimum criterion is utilized [4], [5]. According to the rules of the magnitude optimum, the larger time constant of the controlled system T_l has to be compensated with the controller time constant $T_{N,el}$:

$$T_{N,el} = T_l = \frac{L}{R}. \tag{15}$$

A small time constant T_s is determined by the dead time of power electronics and by additional delays in the control loop, such as signal propagation time and processing time. The dead time is caused by current measurement, which is only triggered twice in a PWM period. Therefore, the small time constant is approximated to the PWM period $T_{PWM} = 1/f_{PWM} = T_s$ [6]. The complete transfer function of the open control structure results in

$$G_{o,el}(s) = K_{P,el} \cdot \frac{T_{N,el}\,s + 1}{T_{N,el}\,s} \cdot \frac{\frac{1}{R}}{T_l\,s + 1} \cdot \frac{1}{T_s\,s + 1}. \tag{16}$$

The controller gain $K_{P,el}$ is calculated such that the absolute value of the reference transfer function is kept close to one for the largest possible frequency range, resulting in

$$K_{P,el} = \frac{T_N}{2\,K_S\,T_E} = \frac{L}{2\,T_s}, \tag{17}$$

where K_S is the static gain of the numerator of the open loop transfer function and T_E the smaller time constant of the transfer function $G_{0,el}$. Consequently, the resulting current transfer function of the closed-loop control is defined as

$$G_{c,el}(s) = \frac{G_{o,el}}{1 + G_{o,el}} = \frac{1}{2\,T_s\,s\,(1 + T_s\,s) + 1}. \tag{18}$$

B. Mechanical Subsystem

The mechanical equation results from the balance of forces with the magnetic force F_{Mag}, the weight force, where m is the mass and g is the gravitational acceleration and the inertial force

$$0 = F_{Mag}(\delta_L, I) - mg + m\ddot{\delta}_L. \tag{19}$$

Because $F_{Mag}(\delta_L, I)$ is nonlinear, the differential equation has to be linearized, to evaluate the controller parameters. The resulting equation is split into a static and a dynamic equation. The static equation is defined as

$$F_{Mag}(I_0, \delta_{L,0}) = m \cdot g. \tag{20}$$

The actuator was designed in such a way, that the weight force is compensated by the force, generated by the permanent magnet (see sec. III), therefore the static current is set to $I_0 = 0\,\mathrm{A}$. The remaining difference can be seen as a control deviation and is adjusted with the dynamic controller. The dynamic equation is simplified to

$$0 = F_{Mag}(I, \delta_L) + m\,\ddot{\delta}_L. \tag{21}$$

The nonlinear differential equation is linearized to

$$0 = k_{I,Mag}\,\Delta I + k_{\delta,Mag}\,\Delta\delta_L + m\Delta\ddot{\delta}_L, \tag{22}$$

where the current and air gap difference are defined as $\Delta I = I - I_0$ and $\Delta\delta_L = \delta_L - \delta_{L,0}$. The static air gap is defined as the design air gap $\delta_{L,0} = 1.0\,\mathrm{mm}$ (see sec. III). The constant factors $k_{I,Mag}$ and $k_{\delta,Mag}$ result from the magnetic force linearization in the operating point.

$$k_{I,Mag} = \frac{A_{PM} \cdot N \cdot \mu_{r,PM} \cdot (I_0 \cdot N \cdot \mu_0 \cdot \mu_{r,PM} + 2 \cdot B_R \cdot h_{PM})}{2 \cdot (h_{PM} + \delta_{L,0} \cdot \mu_{r,PM})^2} \tag{23}$$

$$k_{\delta,Mag} = -\frac{A_{PM} \cdot \mu_{r,PM} \cdot (I_0 \cdot N \cdot \mu_0 \cdot \mu_{r,PM} + 2 \cdot B_R \cdot h_{PM})^2}{2 \cdot \mu_0 \cdot (h_{PM} + \delta_{L,0} \cdot \mu_{r,PM})^3} \tag{24}$$

With the Laplace Transformation the resulting transfer function of (22) is

$$G_A(s) = \frac{-k_{I,Mag}}{k_{\delta,Mag} + m\,s^2}. \tag{25}$$

From (25) follows that the mechanical system is unstable with poles at $s_{1/2} = \pm\sqrt{\frac{-k_{\delta,Mag}}{m}}$. To reach an asymptotically stable system condition, all poles have to be in the left half of s-plane.

In contrast to the physical system, the desired system behavior is equal to a second order mechanical differential equation following the dynamic of a mass, which is mounted on a spring-damper-element with damping constant d and spring constant c.

$$0 = m\,\Delta\ddot{\delta}_L + d\,\Delta\dot{\delta}_L + c\,\Delta\delta_L \tag{26}$$

Thus, (22) is equated with (26). The resulting equation (27) describes the relation between the current and the spring-damper-element and therefore the mechanical behavior of the system.

$$\Delta I = \frac{d}{k_{I,Mag}}\,\Delta\dot{\delta}_L + \frac{c - k_{\delta,Mag}}{k_{I,Mag}}\,\Delta\delta_L \tag{27}$$

With the Laplace Transformation the corresponding transfer function is

$$G_\delta(s) = \frac{\Delta\delta_L}{\Delta I} = \frac{\frac{k_{I,Mag}}{c - k_{\delta,Mag}}}{\frac{d}{c - k_{\delta,Mag}}\,s + 1} = \frac{K_{mech}}{T_{mech}\,s + 1}, \tag{28}$$

where K_{mech} is the static gain and T_{mech} is the time constant of the mechanical system. To compensate the transfer behavior, an ideal PD controller $G_{PD}(s)$ is introduced. The aim is to achieve a transfer behavior of the controlled open loop transfer function such that $G_{PD}(s) \cdot G_\delta(s) = 1$.

$$G_{PD}(s) = \frac{1}{G_\delta(s)} = K_{PD}\,(T_V\,s + 1) \tag{29}$$

This leads to the resulting parameters of the PD controller:

$$K_{PD} = \frac{1}{K_{mech}} = \frac{c - k_{\delta,Mag}}{k_{I,Mag}}, \tag{30}$$

$$T_V = T_{mech} = \frac{d}{c - k_{\delta,Mag}}. \tag{31}$$

In the next step, the closed loop transfer function is investigated to determine the stability of the system. As a simplification, the electrical closed loop transfer function (18) is neglected, due to the fact that the large time constant of the electrical subsystem T_l is considerably smaller, than the time constant of the mechanical subsystem T_{mech}. Therefore, the open loop transfer function of the mechanical system is defined by

$$G_{o,PD}(s) = G_{PD}(s)\,G_A(s) = \frac{-k_{I,Mag}\,K_{PD}\,(T_V\,s + 1)}{m\,s^2 + k_{\delta,Mag}}. \tag{32}$$

The corresponding closed loop transfer function is determined to

$$G_{c,PD}(s) = \frac{G_{o,PD}(s)}{1 + G_{o,PD}(s)} = \frac{-k_{I,Mag}\,K_{PD}\,(T_V\,s + 1)}{m\,s^2 + k_{\delta,Mag} - k_{I,Mag}K_{PD}T_V\,s - k_{I,Mag}K_{PD}} \tag{33}$$

with the poles at

$$s_{1,2} = \frac{k_{I,Mag}K_{PD}T_V}{2\,m} \pm \sqrt{\left(\frac{k_{I,Mag}K_{PD}T_V}{2\,m}\right)^2 - \frac{k_{\delta,Mag} - k_{I,Mag}\,K_{PD}}{m}}. \tag{34}$$

To avoid an oscillating behavior, a double pole in the left half of the s-plane is intended. Therefore, the square root of (34) has to be zero. This is achieved by inserting K_{PD} and T_V to formulate a relation between d and c

$$d = -\sqrt{4\,m\,(2\,k_{\delta,Mag} - c)}, \tag{35}$$

where $c < 2\,k_{\delta,Mag}$ needs to be fulfilled. According to this constraint, the value of c has to be chosen and thus determines the location of the poles.

If the desired value $\Delta\delta_L$ is not zero, then there will be a constant deviation between reference value and actual value. This is caused by the nonlinearity of the differential equation, especially the magnetic force (see (19)). Thus, the PD controller is replaced by a PID controller, to compensate the remaining deviation between reference and actual value. An ideal PID controller has the following structure

$$G_{PID}(s) = K_{PID}\left(1 + \frac{1}{T_N\,s} + T_V\,s\right). \tag{36}$$

The characteristics of the PD part of the PID controller has to be the same as for the PD controller. Therefore, K_{PID} is set to

$$K_{PID} = K_{PD} = \frac{c - k_{\delta,Mag}}{k_{I,Mag}}. \tag{37}$$

The new open loop transfer function out of (25) and (36) is

$$G_{o,PID}(s) = \frac{-k_{I,Mag}K_{PID}\left(1 + \frac{1}{T_N\,s} + T_V\,s\right)}{m\,s^2 + k_{\delta,Mag}}. \tag{38}$$

To achieve stable system behavior, the poles of the closed loop transfer function of (38) have to be determined. The

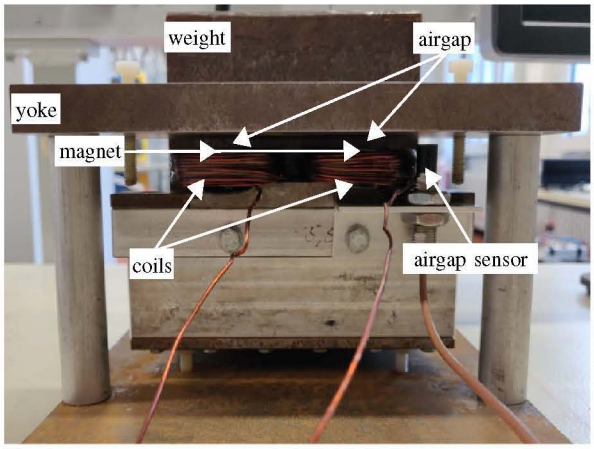

Fig. 6: Test bench for hybrid actuator validation.

selection of the reset time T_N is then dependent on the trade off between overshooting and duration until control deviation is compensated. In this case a well damped system behavior is reached by setting T_N as a multiple of T_{mech}. Therefore, T_N is selected to 80 ms.

V. Validation

For the validation of the discussed controller the hybrid actuator test bench in Fig. 6 is used. It consists of the hybrid actuator, an iron yoke, an air gap sensor and an iron weight of 6 kg. The actuator can oscillate freely within an adjustable range, set to 0.5 mm - 1.5 mm during operation.
The control algorithm is implemeted on a $ST\ Nucleo - F767ZI$ microcontroller (MCU) (Fig. 7a). For air gap- and current measurement a shield board (Fig. 7b) is designed. The shield is mounted on the MCU and equipped with a 16-channel 16-Bit dual simultaneous sampling ADC ($Analog\ Devices\ AD7616$) exchanging data with the MCU via SPI. Apart from that, the power supply and PWM outputs as well as measurement inputs for six H-bridges are part of the shield board. The H-bridge in Fig. 7c is equipped with two half bridges of type $International\ Rectifier\ IRSM808 - 204MH$ and a $LEM\ LAX\ 100 - NP$ for current measurement. Additionally, electronics for air gap measurement and power supply of the air gap amplifier are part of the board. Air gap measurement is realized with an eddy current sensor and amplifier of type $Emerson\ PR6423$ and $Emerson\ CON021$.

(a) STM32F767ZI (b) Nucleo Shield (c) H-bridge

Fig. 7: Hardware for controller implementation and validation.

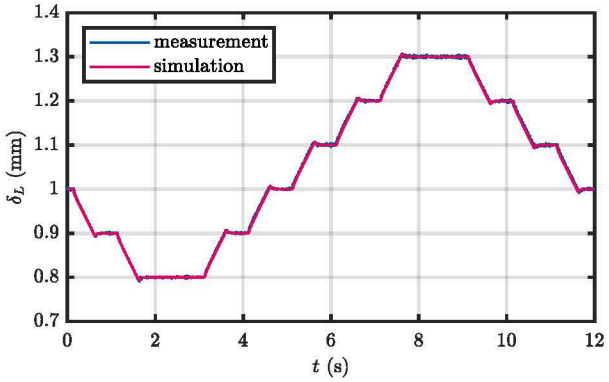

(a) Air gap measurement.

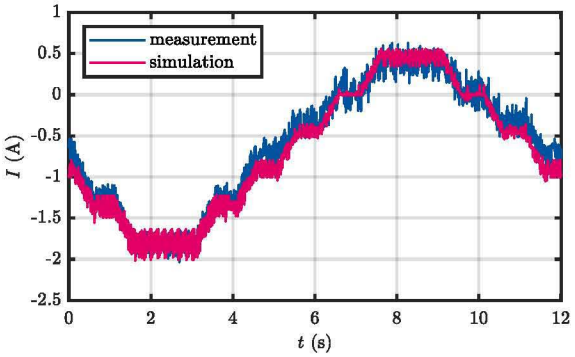

(b) Current measurement.

Fig. 8: Comparison of measurement and simulation for an air gap gradient of 0.2 mm/s.

A. Simulation

Simulation is performed numerically in $Simulink$. For this purpose a model is implemented following the structure in Fig. 5. The hybrid actuator is modeled according to the mechanical differential equation (19). Dependency between magnetic force and current is given in (9). For power electronics simulation, $PLECS$ is used. All relevant parameters can be taken from table I.

B. Comparison of simulation and measurement

In Fig. 8 measurement and simulation results are shown for an air gap gradient of 0.2 mm/s and in Fig. 9 for 2 mm/s. The ramp starts at 1.0 mm air gap and continues to 0.8 mm as a minimum and 1.3 mm as maximum in 0.1 mm steps.
It can be summarized, that the air gap simulation and measurement fit very closely for both air gap gradients. Only the overshoots at a gradient of 2 mm/s are slightly more distinct. The mean air gap deviation between simulation and measurement for 0.2 mm/s is 0.0022 mm and for 2 mm/s is 0.0038 mm.
Because simulation is based on a lumped parameter model in one operating point, it cannot represent complex physical behavior of the test bench, which leads to current deviations. The mean current deviation between simulation and measurement for 0.2 mm/s is 0.14 A and for 2 mm/s is 0.16 A.

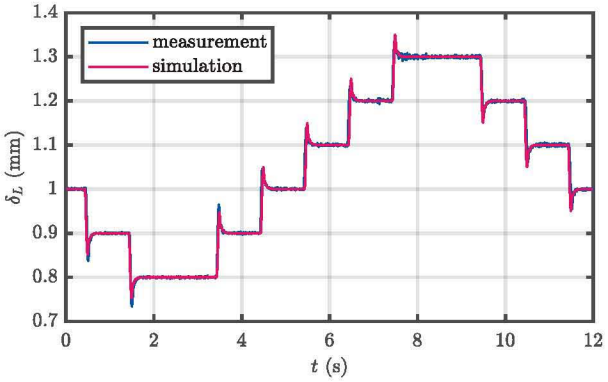

(a) Air gap measurement.

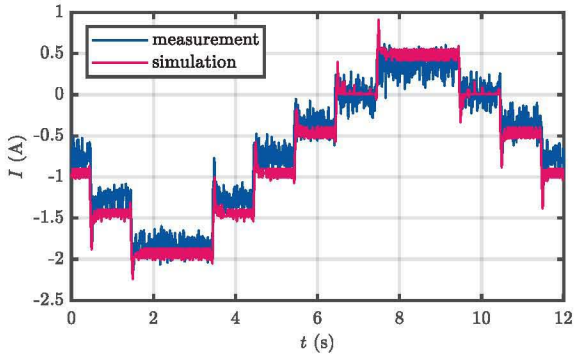

(b) Current measurement.

Fig. 9: Comparison of measurement and simulation for an air gap gradient of $2\,\mathrm{mm/s}$.

TABLE I: Simulation and measurement parameters.

Parameter	Unit	Value
General		
DC link voltage U_{dc}	V	30
PWM frequency f_{PWM}	kHz	10
Hybrid actuator		
Magnet		NdFeB N35 20x20x1 mm
N	-	2x70=140
R @ 10 kHz	Ω	1.064
L @ 10 kHz	mH	0.389
Operating point in simulation		
$\delta_{L,0}$	mm	1.0
m	kg	5.15
B_R	T	0.90
Current controller		
$K_{P,el}$	Ω	1.945
$T_{N,el}$	ms	0.366
Air gap controller		
K_{PID}	kA/m	-12.48
T_N	ms	80
T_V	ms	8.9
System characteristics		
Damping constant d	kg/s	-1394
Spring constant c	N/m	$-0.21997 \cdot 10^6 = 3.5 \cdot k_{\delta,Mag}$
Time constant T_{mech}	ms	8.9

VI. Conclusions

In this paper a hybrid actuator for a Maglev train model is presented. The analytical calculation of a magnetic circuit consisting of iron yoke, air gap, permanent magnets and electromagnets is described and the total magnetic force in dependency of current and air gap is deduced. Afterwards the design of the hybrid actuator is explained with a focus on the characteristic of a permanent magnet regarding temperature and demagnetization.

Subsequently the process of current and air gap controller design is discussed to reach asymptotic stability for the closed control loop. This is achieved by adding a PD-controller to the unstable, mechanical differential equation of the magnetic circuit in a way, that the resulting mechanical system can be described by the differential equation of a damped harmonic oscillator whose characteristic parameters are adjustable by calculating parameters of the PD-controller, resulting in the desired system behavior. In a second step, the PD-controller is extended to a PID-controller to avoid deviation between reference and actual value.

In a final step, the hybrid actuator is validated by simulation and on a test bench, therefore air gap and current measurement are compared. The air gap fits very well for different reference values, while the current slightly differs. The simulation parameters belong to the designed operating point regarding load and remanence flux density which reduces simulation accuracy for other operational points. Therefore, simulation can be improved by FE methods to reproduce nonlinear behavior.

Acknowledgment

The authors would like to thank master student Oliver Knie and PCB designer Jörg Paustenbach for supporting the work.

References

[1] G. Bohn and G. Steinmetz, "The electromagnetic levitation and guidance technology of the 'transrapid' test facility Emsland," *IEEE Transactions on Magnets*, Vol. 20, No. 5, Sep. 1984.

[2] V. Jung, *Magnetisches Schweben*, Heidelberg, Germany: Springer-Verlag Berlin Heidelberg, 1988.

[3] H. Cho, J. Yu, S. Jang, C. Kim, J. Lee, H. Han, "Equivalent magnetic circuit based levitation force computation of controlled permanent magnet levitation system," *IEEE Transactions on Magnets*, Vol. 48, No. 11, Nov. 2012.

[4] K. G. Papadopoulos, *PID Controller Tuning Using the Magnitude Optimum Criterion*, Cham, Switzerland: Springer International Publishing, 2015.

[5] D. Schröder, *Elektrische Antriebe - Regelung von Antriebsystemen*, Heidelberg, Germany: Springer-Verlag Berlin Heidelberg, 2015.

[6] M. H. Bierhoff and F. W. Fuchs, "Active damping for three-phase PWM rectifiers with high-order line-side filters", *IEEE Transactions on Industrial Electronics*, Vol. 56, no. 2, pp. 371-379, Feb. 2009.